

The Signal Multi-Vector

Lennart Wietzke · Gerald Sommer

Published online: 11 March 2010
© Springer Science+Business Media, LLC 2010

Abstract This work covers a fundamental problem of local phase based image analysis: the isotropic generalization of the classical 1D analytic signal to two dimensions. The analytic signal enables the analysis of local phase and amplitude information of 1D signals. Local phase, amplitude and additional orientation information can be extracted by the 2D monogenic signal with the restriction to intrinsically 1D signals. In case of 2D image signals the monogenic signal enables the rotationally invariant analysis of lines and edges. In this work we present the 2D analytic signal as a novel generalization of both the analytic signal and the 2D monogenic signal. In case of 2D image signals the 2D analytic signal enables the isotropic analysis of lines, edges, corners and junctions in one unified framework. Furthermore, we show that 2D signals are defined on a 3D projective subspace of the homogeneous conformal space which delivers a descriptive geometric interpretation of signals providing new insights on the relation of geometry and 2D image signals. Finally, we will introduce a novel algebraic signal representation, which can be regarded as an alternative and fully isomorphic representation to classical matrices and tensors. We will show the solution of isotropic intrinsically 2D image analysis without the need of steering techniques.

Keywords Algebraic image analysis · Isotropic local phase based signal processing · Analytic signal · Monogenic signal · Weyl-projection · Structure multi-vector ·

L. Wietzke (✉)
Raytrix GmbH, Schauenburgerstrasse 116, 24118 Kiel, Germany
e-mail: Lennart.Wietzke@raytrix.de

G. Sommer
Cognitive Systems Group, Department of Computer Science, Kiel University, Christian-Albrechts-Platz 4, 24118 Kiel, Germany
e-mail: gs@ks.informatik.uni-kiel.de

Geometric algebra · Clifford analysis · Generalized Hilbert transform · Riesz transform · Conformal space · Projective/homogeneous space · Hybrid matrix geometric algebra · Poisson scale space · Rotational invariance · Radon transform

1 Introduction

Low level two-dimensional image analysis is often the first step of many computer vision tasks. Therefore, local signal features with geometrical and structural information determine the quality of subsequent higher level processing steps. It is important not to lose or to merge any of the original signal information within the local neighborhood of the test point. The constraints of local signal analysis are: to span an orthogonal feature space (split of identity) and to be robust against stochastic and deterministic deviations between the actual signal and the assumed signal model. One of the fundamental problems in image analysis is a good signal representation. Such a structural signal feature is the local phase information which is robust with respect to noise, contrast and illumination changes [9, 10, 18]. In case of image signals it is shown in [23] that the original signal can be recovered to a fairly large extent by using only its phase information while setting its amplitude information to unity. In contrast to that, if only the amplitudes are obtained and the phases are set to zero, the recovered image signal is completely indiscernible. Therefore, phase based signal processing has found success in many applications, such as disparity estimation of stereo [10], matching [2], face recognition [35], optical flow estimation [36], demodulation of fringe patterns [21], and in medical image analysis [14, 15].

Many low-level approaches such as the SIFT features are based on derivatives. In this work we will substitute those

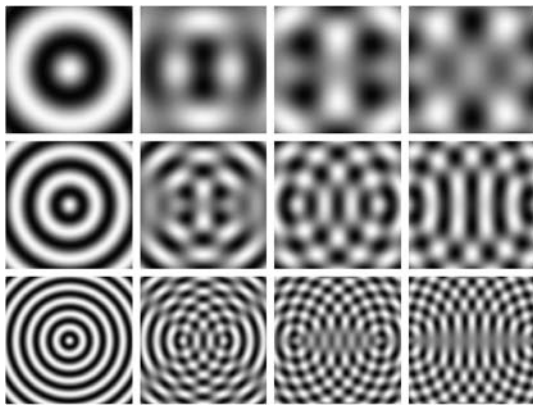


Fig. 1 Interference of two waves. From top to bottom: increasing frequency. From left to right: increasing wave center distance. Signal analysis task: at each location the two waves have to be separated from each other

derivatives by their analog components of the generalized Hilbert transforms. In Fourier space $\mathcal{F}\{f\}(u) = \hat{f}(u)$ [20] it can be seen clearly that the derivative operator of order m , \mathcal{D}_m ,

$$\mathcal{F}\{\mathcal{D}_m\{f\}\}(u) = (2\pi u \mathbf{i})^m \hat{f}(u) \tag{1}$$

with $u \in \mathbb{R}^2$ is closely related to the generalized Hilbert transform operator

$$\mathcal{F}\{\mathcal{H}_m\{f\}\}(u) = (2\pi \bar{u} \mathbf{i})^m \hat{f}(u) \tag{2}$$

with $\bar{u} = \frac{u}{\|u\|}$. This work is organized as follows: we will generalize the analytic signal step by step. First we will give an introduction to one-dimensional signal analysis with the classical analytic signal which is a complex-valued signal extension. The analytic signal is based on the Hilbert transform which will be generalized to multiple dimensions. We will proceed with the 2D monogenic signal which is a vector-valued signal representation, and defined on 2D domains but restricted to intrinsically one-dimensional signals. This drawback will be solved in this work. The 2D monogenic signal will be generalized to a certain subclass of 2D signals by the so called isotropic 2D analytic signal, which is a signal representation embedded in projective space. The most generalized form will be given at the end of this work by the so called signal multi-vector, which is a signal extension embedded in a subspace of the 32-dimensional conformal space. All signal analysis solutions presented in this work are truly isotropic, i.e. no steering technique or explicit Radon transform must be used. This advantage offers most accuracy in less computational time since only a small filter set must be applied to the original signal.

Applications of the results presented in this work are the isotropic separation of superimposed structures as shown in Fig. 1.

2 The Classical 1D Analytic Signal

To solve phase based 2D signal analysis problems, first phase based 1D signal analysis has to be considered. From Fourier analysis it is well known that each 1D signal $f \in L^2(\mathbb{R}) \cap L^1(\mathbb{R})$ can be approximated globally with infinite small error by its Fourier series

$$f(x) = \sum_v a_v \cos(v(x + \phi_v)) \tag{3}$$

with v as the frequency. Each frequency component with its appropriated individual phase ϕ_v and amplitude a_v can be analyzed separately. This selected frequency of interest carries the structural information of the signal and has to be extracted from the original signal by applying a filter kernel $p_s : \mathbb{R}^2 \mapsto \mathbb{R}$ before analysis. Therefore, the local 1D signal model at the origin $x = 0$ in the applied local coordinate system reads

$$f^e(x, s) = a(x, s) \cos \phi(x, s) = (p_s * f)(x) \tag{4}$$

with $*$ as the 1D convolution operator, and $s > 0$ as the scale space parameter of a filter kernel p_s , which will be specified later. Since the local signal model is assumed to be an even function, i.e.

$$\cos(x) = \cos(-x) \quad \forall x \in \mathbb{R}, \tag{5}$$

it is called the even part f^e of the analytic signal. By means of convolution of the filtered original signal with the classical first order 1D Hilbert transform kernel

$$h(\tau) = \frac{1}{\pi \tau} \tag{6}$$

the corresponding odd part f^o can be calculated by

$$f^o(x, s) = a(x, s) \sin \phi(x, s) = (h * p_s * f)(x) \tag{7}$$

and

$$(h * p_s * f)(x) = \text{P.V.} \int_{\mathbb{R}} \frac{(p_s * f)(x - \tau)}{\pi \tau} d\tau \tag{8}$$

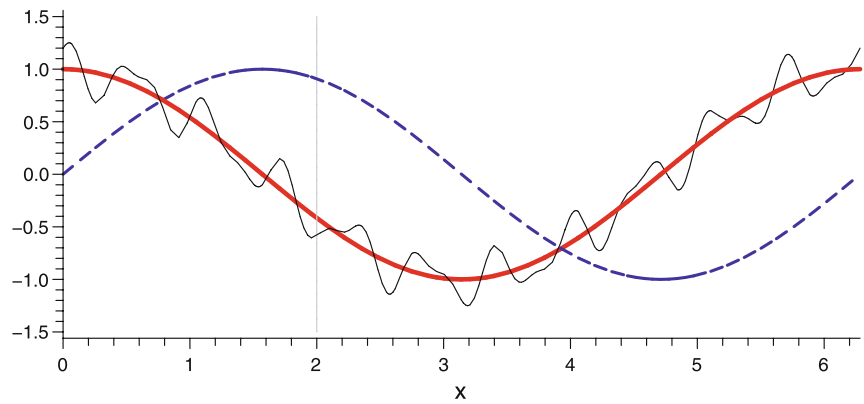
as the classical 1D Hilbert transform of the signal f in scale space and P.V. as the Cauchy principal value. Since the Hilbert transform of the original signal is locally an odd function, i.e.

$$\sin(x) = -\sin(-x) \quad \forall x \in \mathbb{R}, \tag{9}$$

it is called the *odd part* f^o of the analytic signal. One important local structural feature of the filtered signal is the local phase $\phi(x, s) \in [0, 2\pi)$ [19] because it is independent of the local signal amplitude $a(x, s)$ [13]. The local phase can be determined by

$$\phi(x, s) = \arctan \frac{f^o(x, s)}{f^e(x, s)} \tag{10}$$

Fig. 2 Illustration of the original (*thin plot*) 1D signal and its even f^e (*thick plot*) and odd f^o (*dashed plot*) signal parts in scale space (for the frequency component $\nu = 1$ Hz) with local structural amplitude $a(2, s) = 1$ and phase $\phi(2, s) = 2$ at the test point $x = 2$. It can be seen clearly that the even signal part carries the main structural information of the original signal



and the local signal amplitude can be determined by

$$a(x, s) = \sqrt{(f^e(x, s))^2 + (f^o(x, s))^2}. \tag{11}$$

The local phase information is called structural signal information. The vector valued signal extension

$$[f^e(x, s), f^o(x, s)]^T \tag{12}$$

of a scalar valued one-dimensional signal f is called analytic signal, see Fig. 2. Note that originally the analytic signal has been defined as a complex valued signal with f^e as the real part and f^o as the imaginary part [11], i.e.

$$f^a(x, s) = f^e(x, s) + \mathbf{i}f^o(x, s). \tag{13}$$

The 1D analytic signal has been used also in 2D signal processing. This makes it necessary to extend the classical 1D Hilbert transform to multiple dimensions. There are several approaches in the literature which lack the required rotational invariance of the multidimensional Hilbert transform, see [1, 16]. The partial Hilbert transform is such a naive ansatz of applying the one-dimensional Hilbert transform to two-dimensional signals $f \in L^2(\mathbb{R}^2) \cap L^1(\mathbb{R}^2)$

$$(h * f_\theta)(t) = \text{P.V.} \int_{\mathbb{R}} \frac{f((\tau + t) \cos \theta, (\tau + t) \sin \theta)}{\pi \tau} d\tau \tag{14}$$

with the partial two-dimensional function in direction θ at the origin of the applied local coordinate system reads

$$f_\theta(\tau) = f(\tau \cos \theta, \tau \sin \theta). \tag{15}$$

In case the main orientation of the 2D signal is unknown, the partial Hilbert transform has to be executed in all possible directions. Of course, exact approaches must not try all of these directions. One possible rotationally invariant generalization of the one-dimensional Hilbert transform to higher dimensions is the Riesz transform which will be called generalized Hilbert transform in the following.

3 The Isotropic 2D Analytic Signal

Based on the results of Fourier theory and functional analysis we assume that each 2D signal $f \in L^2(\mathbb{R}^2) \cap L^1(\mathbb{R}^2)$ can be locally modeled¹ by a superposition of arbitrarily orientated one-dimensional cosine waves [34]

$$(p_s * f)(z) = a(z, s) \sum_{\nu=1}^n \cos(\langle z, \bar{o}_\nu(z, s) \rangle + \phi(z, s)) \tag{16}$$

with $z = (x, y)$, $*$ as the convolution operator and the orientation $\bar{o}_\nu(z, s) = [\cos \theta_\nu(z, s), \sin \theta_\nu(z, s)]^T$. Note that each cosine wave is determined with the same amplitude and phase information. This restriction will be generalized within this work. The Poisson convolution kernel [8] reads

$$p_s(z) = \frac{s}{2\pi(s^2 + \|z\|^2)^{3/2}}, \tag{17}$$

see Fig. 4. For a certain scale space parameter $s \in \mathbb{R}_+$ the Poisson kernel acts as a low pass filter on the original signal f . The Poisson scale space is naturally related to the generalized Hilbert transform by the Cauchy kernel [5].

To filter a frequency interval of interest, the difference of Poisson (DoP) kernel will be used in practice

$$p_{s_f, s_c}(z) = p_{s_f}(z) - p_{s_c}(z) \tag{18}$$

with $s_c > s_f > 0$ and s_c as the coarse scale parameter and s_f as the fine scale parameter. The filtered signal is defined by convolution with the difference of Poisson kernel which will be used to analyze the original signal with the DoP operator to consider only a small passband of the original signal spectrum.

¹There is no method of signal analysis which is universal in respect of any arbitrary local 2D structure. Hence, it is necessary to formulate a model of local signal structure as basis of the analysis. The great challenge is the search for a most general model which can cope with as many as possible local signal structures.

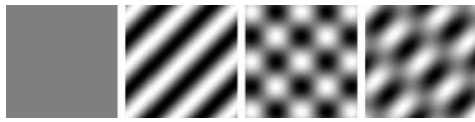


Fig. 3 From left to right: i0D signal, i1D signal with $n = 1$ in (16) to model straight lines and edges in scale space and two i2D signals which consist of two superimposed i1D signals with $n = 2$ in (16) to locally model junctions and corners in scale space

Without loss of generality the signal model in (16) degrades locally at the origin $z = \mathbf{0}$ of a local coordinate system to

$$f_p(z, s) = \sum_{v=1}^n a(z, s) \cos \phi(z, s) \tag{19}$$

In case of image analysis lines, edges, junctions and corners can be modeled in this way. The signal processing task is now to determine the local amplitude $a(z, s)$, the local orientation $\theta_v(z, s)$ and the local phase $\phi(z, s)$ for a certain scale space parameter s and a certain phase location z . This problem has been already solved for one-dimensional signals by the classical analytic signal [11] by means of the Hilbert transform [16] and for intrinsically one-dimensional [37] signals (i.e. $n = 1$ in (16)) by the 2D monogenic signal [7] by means of the generalized first order Hilbert transform.

This work shows that 2D signal processing can be regarded as an inverse problem [33] where higher order generalized 2D Hilbert transforms are applied to the original signal f , here with the signal model in (16) restricted to $n < 3$. 2D signals in scale space are classified into local regions $N \subseteq \Omega$ of different intrinsic dimensions [37] (which correspond to their codimension). The intrinsic dimension expresses the number of degrees of freedom necessary to describe local structure. Constant signals without any structure are of intrinsic dimension zero (i0D), arbitrary orientated straight lines and edges are of intrinsic dimension one (i1D), and all other possible patterns such as corners and junctions are of intrinsic dimension two (i2D), see Fig. 3. In general i2D signals can only be modeled by an infinite number of superimposed i1D signals. Therefore, it is essential to assume a certain signal model or a set of certain models for exact i2D signal analysis. Furthermore, the intrinsic dimension depends also on the scale space parameter s at which the signal will be considered locally.

3.1 Related Work: The Monogenic Signal

Related work is the recently introduced monogenic signal [7] which can be regarded as the Hilbert transform based analogue to the derivative based gradient. The first order generalized Hilbert transform kernel

$$h^{(1)}(z) = \begin{bmatrix} h_x^{(1)} \\ h_y^{(1)} \end{bmatrix} (z) = \frac{1}{2\pi \|z\|^3} \begin{bmatrix} x \\ y \end{bmatrix} \tag{20}$$

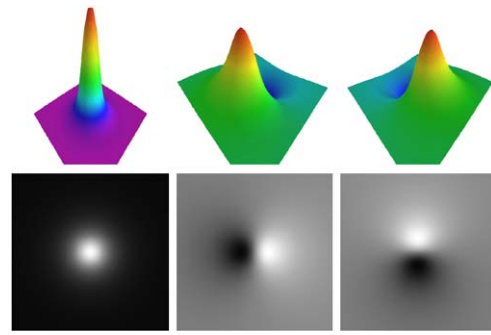


Fig. 4 From left to right: Poisson convolution kernel $p(z, s)$ and conjugate Poisson convolution kernels $q_x^{(1)}(z, s)$ and $q_y^{(1)}(z, s)$ in the spatial domain for a certain scale space parameter $s > 0$

can be expressed in Poisson scale space by

$$q^{(1)}(z, s) = \begin{bmatrix} q_x^{(1)} \\ q_y^{(1)} \end{bmatrix} (z, s) = \begin{bmatrix} p_s * h_x^{(1)} \\ p_s * h_y^{(1)} \end{bmatrix} (z) = \frac{1}{2\pi (s^2 + \|z\|^2)^{3/2}} \begin{bmatrix} x \\ y \end{bmatrix}. \tag{21}$$

The 2D monogenic signal can be defined as a vector valued signal representation $[f_p(z, s), f_x(z, s), f_y(z, s)]^T$ where the first order Hilbert transformed signal can be expressed in Radon space [31] by the relation

$$\begin{bmatrix} f_x \\ f_y \end{bmatrix} (z, s) = \begin{bmatrix} q_x^{(1)}(\cdot, s) * f \\ q_y^{(1)}(\cdot, s) * f \end{bmatrix} (z) = \mathcal{R}^{-1} \left\{ (t, \theta) \mapsto \begin{bmatrix} \cos \theta \\ \sin \theta \end{bmatrix} (h * f_r(\cdot, \theta, s))(t) \right\} (z) \tag{22}$$

with the 2D Radon transform $\mathcal{R}\{\cdot\}$, its inverse $\mathcal{R}^{-1}\{\cdot\}$ and the Hilbert transform kernel² h . The Radon transformed signal (see Fig. 5) equals the line-integral

$$f_r(t, \theta; s) = \mathcal{R}\{p_s * f\}(t, \theta) = \int_{\mathbb{R}} (p_s * f)(\tau(\sin \theta, -\cos \theta) + t(\cos \theta, \sin \theta)) d\tau \tag{23}$$

with $\theta \in [0, \pi)$ as the orientation, and $t \in \mathbb{R}$ as the minimal distance of the line to the origin of the local coordinate

²Both the classical 1D Hilbert transform as well as all generalized Hilbert transforms intrinsically always remain in one-dimension, i.e. in this work the function $f(t) = a \cos(t)$ will be considered and its Hilbert transform $(f * h)(t) = a \sin(t)$ with the property $(f * h * h)(t) = -f(t)$.

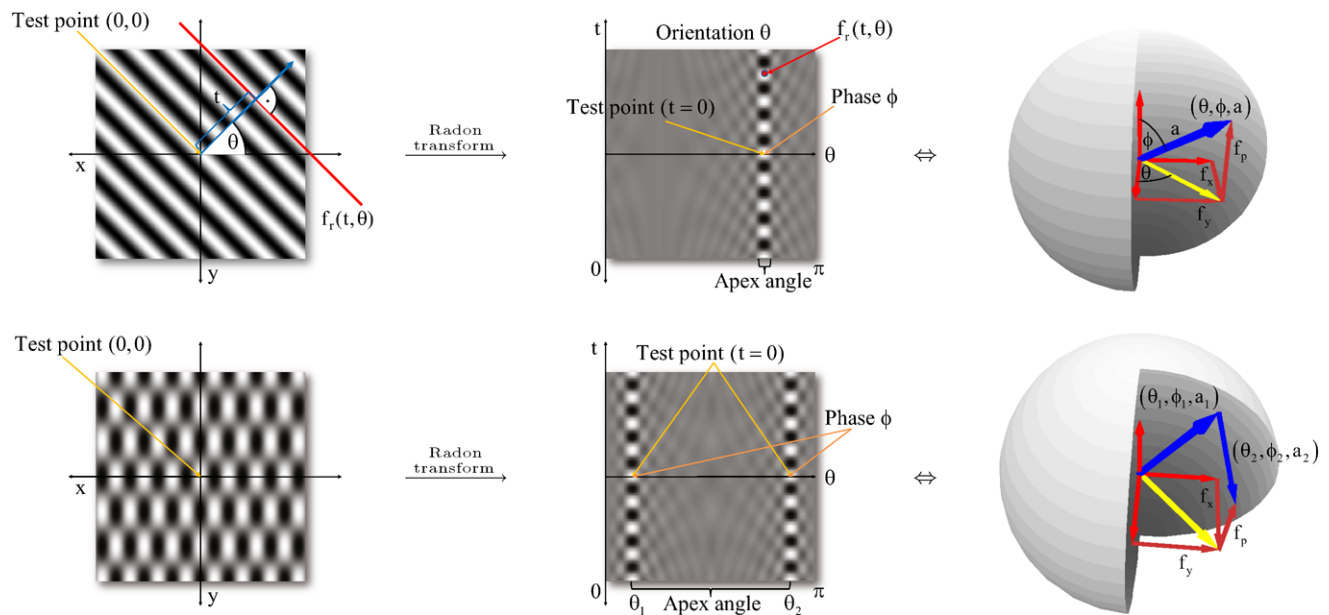


Fig. 5 *Top row* from left to right: illustration of an intrinsically 1D signal in the spatial domain, in its corresponding Radon domain, and its geometric feature interpretation by spherical coordinates $(\theta(z, s), \phi(z, s), a(z, s))$. *Bottom row* from left to right: two superimposed intrinsically 1D signals in the spatial domain modeling locally a

junction. In their corresponding Radon space the two signals are separated from each other into two individual i1D signal slices. The corresponding geometric feature interpretation corresponds to the sum of two vectors with spherical coordinates $(\theta_v(z, s), \phi_v(z, s), a_v(z, s))$ for $v \in \{1, 2\}$

system. The main advantage of this expression in 2D Radon space is the resulting system of equations [31]

$$\begin{bmatrix} f_x \\ f_y \end{bmatrix} (z, s) = \sum_{v=1}^n \begin{bmatrix} \cos \theta_v(z, s) \\ \sin \theta_v(z, s) \end{bmatrix} a(z, s) \sin \phi(z, s) \quad (24)$$

with the explicit formulation of the signal features. This system of equations, together with (19), has to be solved for the unknown signal model features. In case of i1D signals (i.e. $n = 1$ in (16)) this system of equations degrades to

$$\begin{bmatrix} f_p \\ f_x \\ f_y \end{bmatrix} (z, s) = a(z, s) \begin{bmatrix} \cos \phi(z, s) \\ \sin \phi(z, s) \cos \theta(z, s) \\ \sin \phi(z, s) \sin \theta(z, s) \end{bmatrix} \quad (25)$$

which can now be solved for the 3D spherical coordinates, see Fig. 5.

$$\theta(z, s) = \arctan \frac{f_y(z, s)}{f_x(z, s)}, \quad (26)$$

$$\phi(z, s) = \arctan \frac{\sqrt{f_x^2(z, s) + f_y^2(z, s)}}{f_p(z, s)}, \quad (27)$$

$$a(z, s) = \sqrt{f_p^2(z, s) + f_x^2(z, s) + f_y^2(z, s)}. \quad (28)$$

The phase vector $\Phi_{2D}(z, s) \in \mathbb{R}^2$ of the monogenic signal is defined by

$$\Phi_{2D}(z, s) = \begin{bmatrix} \Phi_x \\ \Phi_y \end{bmatrix} (z) = \phi(z, s) \begin{bmatrix} \cos \theta(z, s) \\ \sin \theta(z, s) \end{bmatrix} \quad (29)$$

consisting of the local main orientation $\theta(z, s)$ and the local i1D phase $\phi(z, s)$. The original filtered signal can be reconstructed from the amplitude and phase information by using the definition of the signal model

$$f_0(z, s) = a(z, s) \cos \phi(z, s) + c(z) \quad (30)$$

up to the unknown signals offset $c(z) \in \mathbb{R}$ for all points with intrinsic dimension one. Since the 2D monogenic signal is strictly limited to the class of i1D signals, the aim of this work is to find and solve an appropriate geometrical interpretation for i1D and i2D signals in one single framework.

3.2 Second Order Hilbert Transforms

In case of i2D signals (i.e. $n > 1$ in (16)) the resulting system of equations constructed solely by the first order generalized Hilbert transform in 2D Radon space is not sufficient for the solution of all signal features. Therefore, we have to make use of the higher order generalized Hilbert transforms, such as the second order Hilbert transform kernels [31] (see

Fig. 6

$$q^{(2)}(z, s) = \frac{3s\|z\|^2 + 2s^3 - 2(\|z\|^2 + s^2)^{3/2}}{2\pi\|z\|^4(\|z\|^2 + s^2)^{3/2}} \begin{bmatrix} x^2 \\ xy \\ y^2 \end{bmatrix} \quad (31)$$

(proof: Appendix A) with $z = (x, y)$ and

$$q^{(2)}(z, s) = \begin{bmatrix} q_{xx}^{(2)} \\ q_{xy}^{(2)} \\ q_{yy}^{(2)} \end{bmatrix} (z, s) = \begin{bmatrix} h_x^{(1)} * h_x^{(1)} * p_s \\ h_x^{(1)} * h_y^{(1)} * p_s \\ h_y^{(1)} * h_y^{(1)} * p_s \end{bmatrix} (z) \quad (32)$$

to determine the second order generalized Hilbert transformed signal which can be also expressed in Radon space by

$$\begin{aligned} & \begin{bmatrix} f_{xx} \\ f_{xy} \\ f_{yy} \end{bmatrix} (z, s) \\ &= \begin{bmatrix} q_{xx}^{(2)}(\cdot, s) * f \\ q_{xy}^{(2)}(\cdot, s) * f \\ q_{yy}^{(2)}(\cdot, s) * f \end{bmatrix} (z) \\ &= -\mathcal{R}^{-1} \left\{ (t, \theta) \mapsto \begin{bmatrix} \cos^2 \theta \\ \sin \theta \cos \theta \\ \sin^2 \theta \end{bmatrix} f_r(t, \theta; s) \right\} (z). \quad (33) \end{aligned}$$

Analogously to the first order Hilbert transform the following additional system of equations results from the second order Hilbert transformed signal

$$\begin{aligned} & \begin{bmatrix} f_{xx} \\ f_{xy} \\ f_{yy} \end{bmatrix} (z, s) \\ &= \sum_{v=1}^n \begin{bmatrix} \cos^2 \theta_v(z, s) \\ \frac{1}{2} \sin(2\theta_v(z, s)) \\ \sin^2 \theta_v(z, s) \end{bmatrix} a(z, s) \cos \phi(z, s). \quad (34) \end{aligned}$$

Now a suitable signal structure is required which embeds the original signal extended by the first order and the second order generalized Hilbert transforms in one unified signal representation. This signal representation must be superior for the feature interpretation. Since the signal features are of geometric nature, we are now introducing a geometric algebra signal representation.

3.3 From Tensors to Multi-Vectors

For complete signal analysis problems the original signal has to be extended by the generalized Hilbert transforms. The resulting signal representation can be complex valued, quaternionic valued or tensor valued. When using generalized Hilbert transforms of order two and three or even higher, the extended signal is tensor-valued or matrix-valued

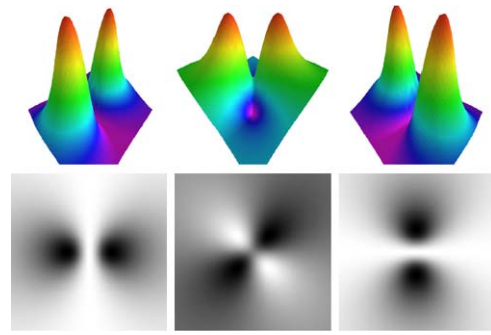


Fig. 6 From left to right: second order Hilbert transform convolution kernels in the spatial domain $q_{xx}^{(2)}(z, s)$, $q_{xy}^{(2)}(z, s)$ and $q_{yy}^{(2)}(z, s)$ for a certain scale space parameter $s > 0$

with multi-vector-valued entries. To analyze such signals geometrically, the matrix or tensor forms have to be mapped to a multi-vector. Such multi-vectors can be interpreted in a geometric way. The objective of the section is to introduce an isomorphic mapping from tensor and matrices to multi-vectors.

The structures of matrix algebra and geometric algebra [17] are completely compatible and in many ways complementary, each having their own advantages and disadvantages. In this section we present a detailed study of the hybrid 2×2 matrix geometric algebra (HMGA) [27]

$$M(2, \mathbb{GA}_3) = \left\{ M = \begin{bmatrix} M_{11} & M_{12} \\ M_{21} & M_{22} \end{bmatrix} : M_{\nu\mu} \in \mathbb{GA}_3 \right\} \quad (35)$$

with elements in the 8-dimensional geometric algebra \mathbb{GA}_3 of Euclidean space. The resulting hybrid structure, which is isomorphic to the geometric algebra $\mathbb{GA}_{4,1}$ of de Sitter space, combines the simplicity of 2×2 matrices and the clear geometric interpretation of the elements of \mathbb{GA} , which will be used in this work for signal analysis.

$$M(2, \mathbb{GA}_3) \cong \mathbb{GA}_{4,1}. \quad (36)$$

It is well known that the geometric algebra $\mathbb{GA}_{4,1}$ contains the 3-dimensional projective, and the conformal space, together with the horosphere of 3-dimensional Euclidean space which has attracted the attention of computer scientists and engineers as well as mathematicians and physicists [25].

In this section we present a novel, fully isomorphic and alternative algebraic representation to tensor and matrix structures, called multi-vector representation, which is very suitable for signal interpretation. It has been shown that the monogenic signal can be analyzed as a vector in Euclidean space. Now a generalized concept of the monogenic signal representation will be presented by analyzing not a vector but a so called multi-vector in conformal space. According to [27] each Clifford number valued matrix $T(z, s) \in M(2, \mathbb{GA}_3)$ with $\mathbb{GA}_3 = \mathbb{GA}(\mathbb{R}^3)$ can be

mapped to a multi-vector $m(z, s) \in \mathbb{G}\mathbb{A}_{4,1}$ of the Clifford algebra [4] $\mathbb{G}\mathbb{A}_{4,1} = \mathbb{G}\mathbb{A}(\mathbb{R}^{4,1})$ with the set of generating basis vectors

$$B = \{\mathbf{e}_1, \mathbf{e}_2, \mathbf{e}_3, \mathbf{e}_+\} \cup \{\mathbf{e}_-\} \tag{37}$$

which results in the total number of $\|2^B\| = 32$ basis multi-vectors with 2^B as the powerset of the set B . The basis vectors have the properties

$$\mathbf{e}_1^2 = \mathbf{e}_2^2 = \mathbf{e}_3^2 = \mathbf{e}_+^2 = 1, \quad \mathbf{e}_-^2 = -1 \tag{38}$$

and

$$\mathbf{e}_i \mathbf{e}_j = -\mathbf{e}_j \mathbf{e}_i, \quad i, j \in \{1, 2, 3, +, -\}, \quad i \neq j. \tag{39}$$

We will use the abbreviation

$$\mathbf{e}_{ij} = \mathbf{e}_i \mathbf{e}_j \tag{40}$$

and in general for the totally ordered set I

$$\mathbf{e}_I = \mathbf{e}_{i_1 i_2 \dots i_n} \quad \text{for } I = \{i_1, i_2, \dots, i_n\} \in 2^B. \tag{41}$$

The scalar numbers \mathbb{R} will be represented by the empty set $I = \emptyset$ with the basis multi-vector $\mathbf{e}_\emptyset = 1$. Note that the basis vector \mathbf{e}_+ extends the three dimensional Euclidean space spanned by $\{\mathbf{e}_1, \mathbf{e}_2, \mathbf{e}_3\}$ to the conformal space and \mathbf{e}_- extends the conformal space to the homogeneous conformal space. In literature the homogeneous conformal space will be often abbreviated by conformal space. Since we use the Clifford algebra for geometric interpretation, Clifford algebra can be called geometric algebra [17]. As a direct result of [27] each Clifford valued 2×2 -matrix of the form

$$T(z, s) = \begin{bmatrix} T_{11} & T_{12} \\ T_{21} & T_{22} \end{bmatrix} (z, s) \in M(2, \mathbb{G}\mathbb{A}_3) \tag{42}$$

can be mapped to its corresponding multi-vector $m = \varphi(T(z, s)) \in \mathbb{G}\mathbb{A}_{4,1}$ in (homogeneous) conformal space [25, 30, 32] by the following isomorphism

$$\varphi(T) = T_{11}u_+ + T_{12}u_+\mathbf{e}_+ + T_{21}^*u_-\mathbf{e}_+ + T_{22}^*u_- \tag{43}$$

with

$$T_{ij}^* = \langle T_{ij} \rangle_0 - \langle T_{ij} \rangle_1 + \langle T_{ij} \rangle_2 - \langle T_{ij} \rangle_3 \tag{44}$$

as the *inversion* of the multi-vector

$$T_{ij} = \sum_{v=0}^3 \langle T_{ij} \rangle_v \in \mathbb{G}\mathbb{A}_3 \tag{45}$$

for $i, j \in \{1, 2\}$ with the grade n projector $\langle \cdot \rangle_n$ [25]

$$\langle m \rangle_n = \sum_{\substack{I \in 2^B \\ \|I\|=n}} m_I \mathbf{e}_I \tag{46}$$

of the multi-vector

$$m = \sum_{I \in 2^B} m_I \mathbf{e}_I \in \mathbb{G}\mathbb{A}_{4,1}, \quad m_I \in \mathbb{R} \tag{47}$$

and

$$u_+ = \frac{1}{2} + \frac{1}{2}\mathbf{e}_{+-}, \tag{48}$$

$$u_- = \frac{1}{2} - \frac{1}{2}\mathbf{e}_{+-}, \tag{49}$$

$$u_+\mathbf{e}_+ = \frac{1}{2}[\mathbf{e}_+ - \mathbf{e}_-] = -\mathbf{e}_0, \tag{50}$$

$$u_-\mathbf{e}_+ = \frac{1}{2}[\mathbf{e}_+ + \mathbf{e}_-] = \frac{1}{2}\mathbf{e}. \tag{51}$$

This results in the general isomorphism

$$\begin{aligned} \varphi(T(z, s)) &= \frac{1}{2}[T_{11}(z, s) + T_{22}^*(z, s)] \\ &\quad + \frac{1}{2}[T_{21}^*(z, s) + T_{12}(z, s)]\mathbf{e}_+ \\ &\quad + \frac{1}{2}[T_{21}^*(z, s) - T_{12}(z, s)]\mathbf{e}_- \\ &\quad + \frac{1}{2}[T_{11}(z, s) - T_{22}^*(z, s)]\mathbf{e}_{+-}. \end{aligned} \tag{52}$$

Since the matrix $T(z, s)$ is isomorphic to the multi-vector $m(z, s)$, the algebra is called a hybrid matrix geometric algebra (HMGA).

The second order partial derivatives of the Hesse matrix of the signal f will be substituted by the second order generalized Hilbert transforms, see (33), in their corresponding directions

$$T^e(z, s) = \begin{bmatrix} f_{xx} & f_{xy} \\ f_{xy} & f_{yy} \end{bmatrix} (z, s) \in M(2, \mathbb{R}) \tag{53}$$

which will be called the even tensor $T^e(z, s)$, see Fig. 7. The resulting isomorphic multi-vector signal representation³ in conformal space reads

$$\varphi(T^e(z, s)) = f_0(z, s) + f_+(z, s)\mathbf{e}_+ + f_{+-}(z, s)\mathbf{e}_{+-} \tag{54}$$

with

$$f_0(z, s) = \frac{1}{2}[f_{xx}(z, s) + f_{yy}(z, s)] = \frac{1}{2}f_p(z, s), \tag{55}$$

$$f_+(z, s) = f_{xy}(z, s), \tag{56}$$

$$f_{+-}(z, s) = \frac{1}{2}[f_{xx}(z, s) - f_{yy}(z, s)] \tag{57}$$

³One of the reviewers notes the relation to the 2-tensor decomposition in irreducible components by $\begin{bmatrix} f_{xx} & f_{xy} \\ f_{xy} & f_{yy} \end{bmatrix} = \frac{f_{xx}+f_{yy}}{2} \begin{bmatrix} 1 & 0 \\ 0 & 1 \end{bmatrix} + \frac{f_{xx}-f_{yy}-2if_{xy}}{4} \begin{bmatrix} -1 & -i \\ -i & 1 \end{bmatrix} + \frac{f_{xx}-f_{yy}-2if_{xy}}{2} \begin{bmatrix} -1 & i \\ i & 1 \end{bmatrix}$.

with $f_0(z, s)$ as the scalar part, $f_+(z, s)$ as the vector part and $f_{+-}(z, s)$ as the so called bivector part of the multi-vector. This multi-vector valued signal representation is constructed by a set of three convolution kernels, see Fig. 8. With the first and second order generalized Hilbert transforms the monogenic signal can now be generalized to the novel 2D analytic signal. Motivated by the important equations (1) and (2), analogous to the Hesse matrix⁴ the second order partial derivatives will be substituted by the second order Hilbert transformed signals in the corresponding directions. This matrix valued signal representation T^e can be mapped to a multi-vector valued signal representation by the isomorphism φ [31], see Fig. 8.

3.4 Signal Interpretation in Projective Space

The local features which determine the signal (16) for the restriction to $n = 2$ and equal amplitude and equal phase in scale space will be separated into geometrical features and structural features. The geometrical features are the main orientation and the rotationally invariant apex angle. The main orientation can be determined by

$$\begin{aligned} \theta_m(z, s) &= \frac{\theta_1(z, s) + \theta_2(z, s)}{2} \\ &= \frac{1}{2} \arctan \frac{f_+(z, s)}{f_{+-}(z, s)}. \end{aligned} \tag{58}$$

In contrast to the monogenic signal the main orientation [26] can be evaluated also at phase positions $\phi(z, s) = k\pi$ for all $k \in \mathbb{Z}$ where the orientation of the monogenic signal

$$\frac{1}{2}[\theta_1(z, s) + \theta_2(z, s)] = \arctan \frac{f_y(z, s)}{f_x(z, s)} \tag{59}$$

is not defined. The apex angle $\alpha(z, s)$ (also known as opening angle or angle of intersection) can be determined by

$$\begin{aligned} \alpha(z, s) &= |\theta_1(z, s) - \theta_2(z, s)| \\ &= \arccos \frac{\sqrt{f_+^2(z, s) + f_{+-}^2(z, s)}}{|f_0(z, s)|} \\ &= \arcsin \frac{\sqrt{f_0^2(z, s) - [f_+^2(z, s) + f_{+-}^2(z, s)]}}{|f_0(z, s)|} \\ &= \arctan \frac{\sqrt{f_0^2(z, s) - [f_+^2(z, s) + f_{+-}^2(z, s)]}}{\sqrt{f_+^2(z, s) + f_{+-}^2(z, s)}} \end{aligned} \tag{60}$$

⁴The first and second order partial derivatives of the Weingarten matrix $[\frac{\partial}{\partial x}, \frac{\partial}{\partial y}, \frac{\partial^2}{\partial x^2}, \frac{\partial^2}{\partial xy}, \frac{\partial^2}{\partial y^2}]^T$ will be substituted by their corresponding generalized Hilbert transforms.

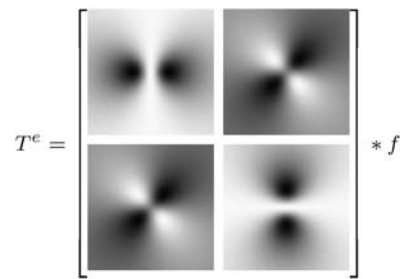


Fig. 7 Illustration of the even tensor T^e which consists of the second order generalized Hilbert transformed signal

$$\varphi(T^e) = \left(\text{[kernel 1]} + \text{[kernel 2]} e_+ + \text{[kernel 3]} e_{+-} \right) * f$$

Fig. 8 Illustration of the isomorphism from the even tensor T^e structure to the multi-vector expression

which delivers in combination with $\theta_m(z, s)$ the individual orientations $\theta_1(z, s)$ and $\theta_2(z, s)$. The apex angle⁵ is a very important rotationally invariant local feature for example it is zero iff the underlying structure is of intrinsic dimension one. The geometric interpretation of the main orientation and the apex angle results from the signal $f_0(z, s)$ which is embedded in 3D space spanned by the representations defined by (55)–(57) as a vector

$$[0, 0, f_0(z, s)]^T \in \mathbb{R}^3. \tag{61}$$

This 3D vector will be rotated by the Euler angles

$$(\alpha(z, s), 2\theta_m(z, s)) \in \left[0, \frac{\pi}{2}\right] \times [0, 2\pi], \tag{62}$$

see Fig. 9. By means of the apex angle $\alpha(z, s)$, a so called homogeneous signal component f_h of the signal f_p in 3D projective space [25] spanned by the vectors f_x, f_y and f_h can now be introduced by

$$f_h(z, s) = \sqrt{\frac{1 + \cos \alpha(z, s)}{2}} \in [0, 1]. \tag{63}$$

In the following a natural relation of the vector valued 2D analytic signal representation and the projective space will be shown. By means of the homogeneous signal component the model based signal features can now be determined. Let be

$$\tilde{f}_x(z, s) = f_h^{-1}(z, s) f_x(z, s) \tag{64}$$

⁵Note that the apex angle of phase based image analysis corresponds to the shape feature of the orthogonal version of the second order derivatives [3] although they are not equal.

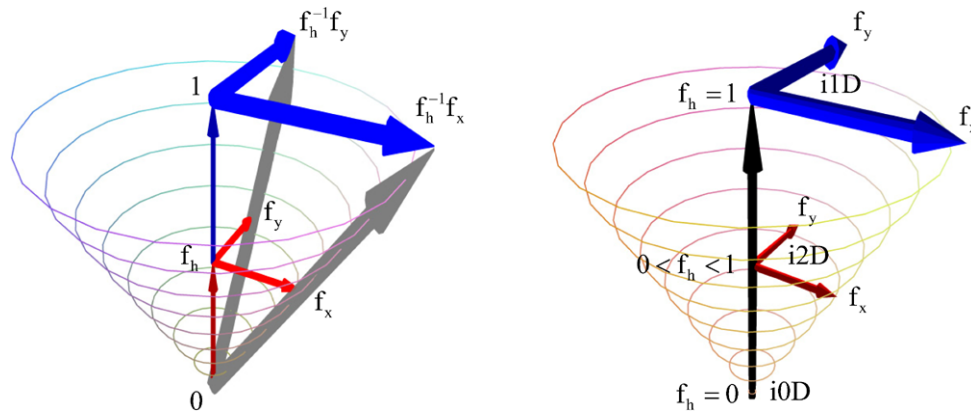


Fig. 9 *Left figure:* the underlying 2D space is spanned by the conjugate signal components f_x and f_y and the additional coordinate of the 3D projective space is given by the homogeneous signal component f_h .

Right figure: illustration of all intrinsic dimensions in one continuous space. The i0D signals are on a point of singularity, the i1D signals can be represented by a 2D plane and the i2D signals exist in a 3D volume

and

$$\tilde{f}_y(z, s) = f_h^{-1}(z, s) f_y(z, s) \tag{65}$$

the normalized signal components of the Hilbert transformed signal. The local main orientation of the signal can be determined by

$$\theta_m(z, s) = \arctan \frac{\tilde{f}_y(z, s)}{\tilde{f}_x(z, s)} \tag{66}$$

which corresponds to (26). The structural signal features are the local phase and the local amplitude. The phase of i1D and i2D signals can be evaluated by

$$\begin{aligned} \phi(z, s) &= \arctan \frac{\sqrt{(\tilde{f}_x(z, s))^2 + (\tilde{f}_y(z, s))^2}}{f_p(z, s)} \\ &= \arctan \frac{\sqrt{f_x^2(z, s) + f_y^2(z, s)}}{f_p(z, s) f_h(z, s)} \end{aligned} \tag{67}$$

which is the generalization of (27) for i1D and i2D signals in one unified framework. The local amplitude for i1D and i2D signals can be determined by

$$a(z, s) = \frac{1}{2} \sqrt{f_p^2(z, s) + (\tilde{f}_x(z, s))^2 + (\tilde{f}_y(z, s))^2} \tag{68}$$

and the local attenuation is given by $\log a$, which is the generalization of (28) for i1D and i2D signals in one unified framework. The phase and the amplitude can be determined by the first order generalized Hilbert transform and the geometric information given by the apex angle and the main orientation can be determined by the second order generalized Hilbert transform. In the case of pure i1D signals the apex angle is zero, i.e. $f_h(z, s) \equiv 1$. In this case the formulas of the phase and amplitude reduce to those known from the

monogenic signal. The advantage of this approach is that it can automatically distinguish between i1D and i2D signals and it can be applied to all kinds of local intrinsic dimension without any previous knowledge about the original signal. In the case of 2D image signals, this approach is designed for an isotropic analysis of lines, edges, corners and junctions in one framework. Note that this analysis is restricted by the assumed signal model. We will overcome these restrictions in the next section. The important generalization from i1D signal analysis to true 2D signal analysis is, that in contrast to the 2D monogenic signal, here the 2D conjugate Poisson components $[f_x, f_y]^T$ are in a natural way located in the higher dimensional 3D projective space $[f_x, f_y, f_h]^T$ with f_h as the additional homogeneous signal component, see Fig. 9. Signal analysis with respect to the local spectral representations amplitude and phase naturally reduces now to the normalization of the homogeneous component to $f_h(z, s) \equiv 1$. This can be easily done by multiplying the conjugate Poisson signal components f_x and f_y by f_h^{-1} . In other words: the 2D space spanned by the signal components f_x and f_y is extended by the homogeneous signal component f_h .

Analogously, the 2D phase vector $\Phi_{2D}(z, s)$ of the 2D monogenic signal can now be generalized to the 3D phase vector $\Phi_{3D}(z, s) \in \mathbb{R}^3$ of the 2D analytic signal, which is defined as

$$\begin{aligned} \Phi_{3D}(z, s) &= \begin{bmatrix} \Phi_x \\ \Phi_y \\ \Phi_z \end{bmatrix} (z, s) \\ &= \phi(z, s) \begin{bmatrix} \cos \theta(z, s) \\ \sin \theta(z, s) \cos \alpha(z, s) \\ \sin \theta(z, s) \sin \alpha(z, s) \end{bmatrix} \end{aligned} \tag{69}$$

consisting of the rotationally invariant local apex angle α , the local main orientation θ and the local i1D/i2D phase ϕ .

In the case of an i1D signal where the apex angle is zero, the 3D phase vector naturally reduces to the phase vector of the 2D monogenic signal.

3.4.1 Proof Outline

Due to the previous results of the first and second order generalized Hilbert transform expressed in Radon space the proofs can now be done by trigonometric calculations using the known local signal components

$$\begin{aligned} & \begin{bmatrix} f_x \\ f_y \\ f_0 \\ f_+ \\ f_{+-} \end{bmatrix} (z, s) \\ &= a(z, s) \\ & \times \begin{bmatrix} [\cos \theta_1(z, s) + \cos \theta_2(z, s)] \sin \phi(z, s) \\ [\sin \theta_1(z, s) + \sin \theta_2(z, s)] \sin \phi(z, s) \\ \cos \phi(z, s) \\ \frac{1}{2}[\sin(2\theta_1(z, s)) + \sin(2\theta_2(z, s))] \cos \phi(z, s) \\ \frac{1}{2}[\cos(2\theta_1(z, s)) + \cos(2\theta_2(z, s))] \cos \phi(z, s) \end{bmatrix} \end{aligned} \tag{70}$$

consisting of five linear independent components which result from the signal intelligence in Radon space. From which follows that

$$\begin{aligned} f_+(z, s) &= a(z, s) \cos \phi(z, s) \\ & \times \cos(\theta_1(z, s) - \theta_2(z, s)) \\ & \times \sin(\theta_1(z, s) + \theta_2(z, s)), \end{aligned} \tag{71}$$

$$\begin{aligned} f_{+-}(z, s) &= a(z, s) \cos \phi(z, s) \\ & \times \cos(\theta_1(z, s) - \theta_2(z, s)) \\ & \times \cos(\theta_1(z, s) + \theta_2(z, s)), \end{aligned} \tag{72}$$

$$\begin{aligned} f_x(z, s) &= 2a(z, s) \sin \phi(z, s) \\ & \times \cos \frac{\theta_1(z, s) - \theta_2(z, s)}{2} \\ & \times \cos \frac{\theta_1(z, s) + \theta_2(z, s)}{2}, \end{aligned} \tag{73}$$

$$\begin{aligned} f_y(z, s) &= 2a(z, s) \sin \phi(z, s) \\ & \times \cos \frac{\theta_1(z, s) - \theta_2(z, s)}{2} \\ & \times \sin \frac{\theta_1(z, s) + \theta_2(z, s)}{2} \end{aligned} \tag{74}$$

and

$$q(z, s) = \sqrt{f_x^2(z, s) + f_y^2(z, s)}$$

$$= 2a(z, s) \sin \phi(z, s) \cos \frac{\theta_1(z, s) - \theta_2(z, s)}{2} \tag{75}$$

from which follows for the main orientation

$$\theta(z, s) = \frac{\theta_1(z, s) + \theta_2(z, s)}{2} \tag{76}$$

that

$$\cos \theta(z, s) = \frac{f_x(z, s)}{\sqrt{f_x^2(z, s) + f_y^2(z, s)}}, \tag{77}$$

$$\sin \theta(z, s) = \frac{f_y(z, s)}{\sqrt{f_x^2(z, s) + f_y^2(z, s)}}. \tag{78}$$

Furthermore

$$\begin{aligned} & \sqrt{f_+^2(z, s) + f_{+-}^2(z, s)} \\ &= a(z, s) \cos \phi(z, s) \cos(\theta_1(z, s) - \theta_2(z, s)) \end{aligned} \tag{79}$$

from which follows for the apex angle $\alpha(z, s)$ that

$$\cos \alpha(z, s) = \sqrt{\left[\frac{f_+(z, s)}{f_0(z, s)}\right]^2 + \left[\frac{f_{+-}(z, s)}{f_0(z, s)}\right]^2} \tag{80}$$

and

$$\sin \alpha(z, s) = \sqrt{1 - \left[\frac{f_+(z, s)}{f_0(z, s)}\right]^2 - \left[\frac{f_{+-}(z, s)}{f_0(z, s)}\right]^2}. \tag{81}$$

Note that the relation to the Radon transform is required solely for interpretation and theoretical results. Neither the Radon transform nor its inverse are ever applied to the signal in practice. Instead, the generalized Hilbert transformed signal components will be determined by 2D convolutions with the generalized Hilbert transform kernels in the spatial domain.

4 The Signal Multi-Vector

We will now present the general solution for isotropic signal analysis in two dimensions. The first step of low level signal analysis is the designation of a reasonable signal model. Based on the fact that signals $f \in L^2(\Omega) \cap L^1(\Omega)$ with $\Omega \subseteq \mathbb{R}^2$ can be decomposed into their corresponding Fourier series, we assume that each frequency component of the original image signal consists locally of a superposition of intrinsically 1D (i1D) [37] signals $f_\nu(z, s)$ with $z = (x, y) \in \mathbb{R}^2$ and $s > 0$, see (82). Each of them is determined by its individual amplitude $a_\nu(z, s) \in \mathbb{R}$, phase $\phi_\nu(z, s) \in [0, \pi)$, and orientation $\theta_\nu(z, s) \in [0, \pi)$.

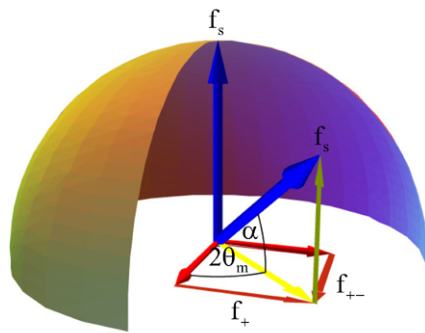
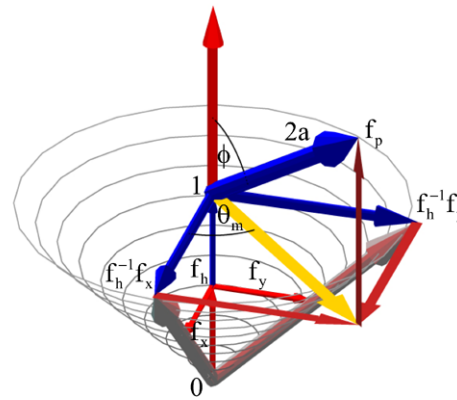


Fig. 10 *Left figure:* geometric interpretation of the main orientation $\theta_m(z, s)$ and the apex angle $\alpha(z, s)$. The 2D analytic signal strictly separates the structural and the geometrical information given by the first and the second order Hilbert transform respectively. *Right figure:*



geometric interpretation of phase $\phi(z, s)$, amplitude $a(z, s)$ and main orientation $\theta_m(z, s)$ in projective space of i1D and i2D signals in one unified framework

4.1 Local Signal Modeling in Scale Space

Applying the Poisson filter kernel p_s to the original signal f results in the smoothed local signal model

$$(p_s * f)(z) = \sum_{v=1}^n a_v(z, s) \cos(\langle z, \bar{o}_v(z, s) \rangle + \phi_v(z, s)) \quad (82)$$

with $\bar{o}_v(z, s) = [\cos \theta_v(z, s), \sin \theta_v(z, s)]^T$ as the oriented normal, and $\langle \cdot, \cdot \rangle$ as the inner product. This powerful local signal model allows modeling any texture or structure such as lines, edges, corners, and junctions in scale space as will be explicitly shows in Sect. 4.3. After having specified the signal model, the mathematical task is the exact retrieval of the signal parameters $(\theta_v(z, s), \phi_v(z, s), a_v(z, s))$ for every position $z \in \Omega$ and for every scale space parameter $s > 0$. In the following

$$f_v^e(z, s) = a_v(z, s) \cos \phi_v(z, s) \quad (83)$$

will be called the even signal part. Furthermore and without loss of generality, at the origin $z = \mathbf{0}$ in the applied local coordinate system, the assumed signal model (82) results in

$$f_p(z, s) = (p_s * f)(z) = \sum_{v=1}^n a_v(z, s) \cos \phi_v(z, s). \quad (84)$$

Since the geometrical information $\theta_v(z, s)$ is not coded in the signal value $f_p(z, s)$, an appropriate signal extension is necessary. Normally, this will be done by calculating higher order derivatives of the signal, e.g. the SIFT features [22]. Instead, in this work the components of the higher order generalized Hilbert transforms will be used.

4.2 Signal Extension

The problem, which has to be solved now, is the search for all unknown structural parameters $a_v(z, s) \in \mathbb{R}$ and

$\phi_v(z, s) \in [0, \pi)$ and the unknown geometric parameters $\theta_v(z, s) \in [0, \pi)$. Although the most general formulas will be provided in this work, we will restrict the signal model (82) to $n < 3$, since by this restriction most signal structures can be modeled [6]. As the signal parameters are unknown, we have to solve a nontrivial inverse problem. This can only be done by extending the original signal representation to result in a system of equations, which includes all unknown signal parameters. This will be done by the generalized Hilbert transforms of higher orders. Our restriction of the signal model to two superimposed arbitrary i1D signals results in six degrees of freedom, which require generalized Hilbert transforms up to order three. The first order generalized Hilbert transform convolution kernels for any dimension read [4]

$$h^{(1)}(z) = \frac{2}{A_{m+1} \|z\|^{m+1}} \begin{bmatrix} z_1 \\ \vdots \\ z_m \end{bmatrix}, \quad z \in \mathbb{R}^m \quad (85)$$

with the area of the unit sphere \mathbb{S}^m in \mathbb{R}^{m+1}

$$A_{m+1} = \frac{2 \pi^{\frac{m+1}{2}}}{\Gamma(\frac{m+1}{2})}. \quad (86)$$

For two-dimensional signals ($m = 2$) the generalized Hilbert transform kernels read

$$\begin{bmatrix} h_x^{(1)} \\ h_y^{(1)} \end{bmatrix}(z) = \frac{1}{2\pi \|z\|^3} \begin{bmatrix} x \\ y \end{bmatrix} \quad (87)$$

which are the analogues to the first order partial derivatives. Since we have to analyze the original signal in scale space, it will be of advantage to provide one unified convolution kernel, which consists of the Poisson kernel and the generalized Hilbert transform kernel of order n . The generalized

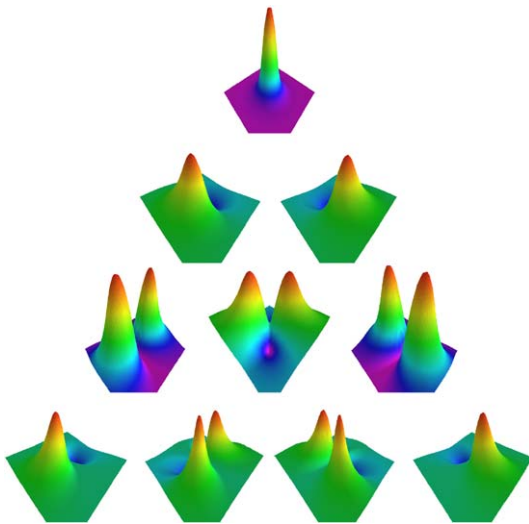


Fig. 11 Illustration from left to right of the convolution kernels in the spatial domain for a certain scale space parameter $s > 0$. *Top row:* Poisson kernel p_s . *Second row:* first order kernels $q_x^{(1)}$ and $q_y^{(1)}$. *Third row:* second order kernels $q_{xx}^{(2)}$, $q_{xy}^{(2)}$ and $q_{yy}^{(2)}$. *Bottom row:* third order kernels $q_{xxx}^{(3)}$, $q_{xxy}^{(3)}$, $q_{xyy}^{(3)}$ and $q_{yyy}^{(3)}$

Hilbert transform kernels of order $(i + j)$ in Poisson scale space reads

$$q_{x^i y^j}^{(i+j)}(z, s) = \underbrace{(h_x^{(1)} * \dots * h_x^{(1)})}_i * \underbrace{(h_y^{(1)} * \dots * h_y^{(1)})}_j * p_s(z) \tag{88}$$

which are shown in Fig. 11. The first order and second order generalized Hilbert transform kernels have been already derived for the 2D analytic signal. The third order generalized Hilbert transform kernels read

$$\begin{bmatrix} q_{xxx}^{(3)} \\ q_{xxy}^{(3)} \\ q_{xyy}^{(3)} \\ q_{yyy}^{(3)} \end{bmatrix} (z, s) = \frac{4s^2(2s^2 + 3\|z\|^2) + 3\|z\|^4 - 8s(s^2 + \|z\|^2)^{3/2}}{2\pi\|z\|^6(s^2 + \|z\|^2)^{3/2}} \times \begin{bmatrix} x^3 \\ x^2y \\ xy^2 \\ y^3 \end{bmatrix}$$

(proof: Appendix B). The value of the $(i + j)$ th order Hilbert transformed signal in Poisson scale space will be derived by convolution in the spatial domain

$$f_{x^i y^j}(z, s) = \left(q_{x^i y^j}^{(i+j)}(\cdot, s) * f \right) (z) \tag{89}$$

Note that for all equations and without loss of generality z always denotes the position relatively to the test point.

4.3 Signal Intelligence in Radon Space

After extending the original signal by the generalized Hilbert transform the resulting signal representation must be interpreted. This can be done in Radon space [31]. The original signal f transformed into Radon space reads

$$\begin{aligned} f_r(t, \theta, s) &= \mathcal{R}\{p_s * f\}(t, \theta) \\ &= \int_{\mathbb{R}^2} (p_s * f)(z) \delta(\langle z, \bar{o}_\theta \rangle - t) dz \end{aligned} \tag{90}$$

with $\theta \in [0, \pi)$ as the orientation, $\bar{o}_\theta = [\cos \theta, \sin \theta]^T$ the oriented normal vector, $t \in \mathbb{R}$ as the minimal distance of the parameterized line to the origin of the local coordinate system of the test point, and δ as the Dirac distribution, see Figs. 5 and 12. The corresponding inverse Radon transform $\mathcal{R}^{-1}\{\cdot\}$ exists, and can be simplified to the following relation for a finite number $n \in \mathbb{N}$ of superimposed 1D signals

$$\begin{aligned} \mathcal{R}^{-1}\{f_r\}(z) &= \frac{1}{2\pi^2} \int_{\theta \in [0, \pi)} \text{P.V.} \int_{t \in \mathbb{R}} \frac{\frac{\partial}{\partial t} f_r(t, \theta; s)}{\langle z, \bar{o}_\theta \rangle - t} dt d\theta \\ &= -\frac{1}{2\pi^2} \sum_{v=1}^n \text{P.V.} \int_{t \in \mathbb{R}} \frac{\frac{\partial}{\partial t} f_r(t, \theta_v; s)}{t} dt \\ &= -\frac{1}{2\pi} \sum_{v=1}^n \text{P.V.} \int_{t \in \mathbb{R}} \frac{1}{\pi t} \frac{\partial}{\partial t} f_r(t, \theta_v; s) dt \\ &= -\frac{1}{2\pi} \sum_{v=1}^n \frac{\partial}{\partial t} (h * f_r(\cdot, \theta_v, s))(t) \end{aligned} \tag{91}$$

with h as the first order one-dimensional Hilbert transform kernel at position $z = \mathbf{0}$ for the origin of the applied local coordinate system, see Fig. 13. The $(i + j)$ th order generalized Hilbert transformed signal can be expressed in Radon space, which delivers a system of equations including all unknown signal parameters. This system of equations can be solved, which was up to now only possible for $n = 1$ in (82) [6]. The Hilbert transformed signal can be expressed by

$$\begin{aligned} f_{x^i y^j}(z, s) &= \mathcal{R}^{-1} \left\{ (t, \theta) \mapsto \cos^i \theta \sin^j \theta (h^{(i+j)} * f_r(\cdot; \theta, s))(t) \right\} (z). \end{aligned} \tag{92}$$

The proof can be done by means of the Fourier slice theorem [31]

$$\mathcal{F}_1\{f_r(\cdot, \theta; s)\}(\rho) = \mathcal{F}_2\{p_s * f\}(\rho \cos \theta, \rho \sin \theta) \tag{93}$$

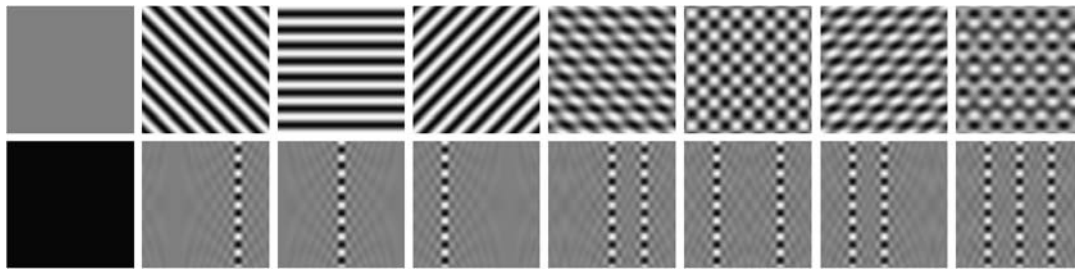
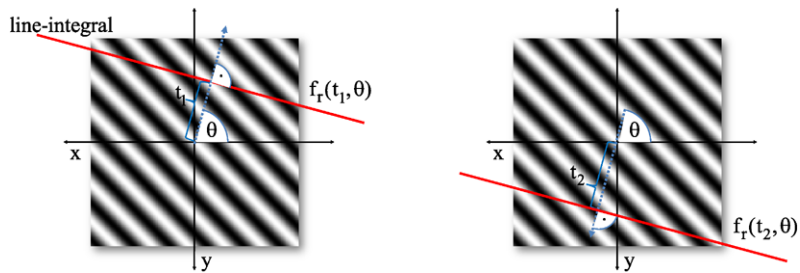


Fig. 12 Top row: illustration of all elements of the powerset of three superimposed intrinsically 1D signals in the spatial domain. From left to right: one constant signal (i0D), three i1D signals with orientation 45°, 90° and 135° followed by four i2D signals which consist of super-

imposed i1D signals. In case of i2D signals the single orientations can hardly be separated in the spatial domain. This can be done much easier in their corresponding Radon domain which is shown in the bottom row

Fig. 13 For each distance parameter t and for all orientations θ —except for the main orientation θ_m —the line-integral on all function values in the signal domain is the same, i.e. $f_r(t_1, \theta; s) = f_r(t_2, \theta; s) \forall t_1, t_2 \in \mathbb{R} \forall \theta \in [0, 2\pi) \setminus \{\theta_m\}$



with \mathcal{F}_m as the m -dimensional Fourier transform. The classical one dimensional Hilbert transform kernel h [16] of order m reads

$$h^{(m)}(t) = \begin{cases} \delta(t), & m \bmod 4 = 0 \\ \frac{1}{\pi t}, & m \bmod 4 = 1 \\ -\delta(t), & m \bmod 4 = 2 \\ -\frac{1}{\pi t}, & m \bmod 4 = 3 \end{cases}, \quad t \in \mathbb{R} \quad (94)$$

with δ as the Dirac distribution, which is the algebraically neutral element of the convolution. Finally, the $(i + j)$ th Hilbert transformed signal results in

$$f_{x^i y^j}(z, s) = \sum_{v=1}^n \cos^i \theta_v(z, s) \sin^j \theta_v(z, s) f_v^{(i+j)}(z, s) \quad (95)$$

because of the property

$$\frac{\partial}{\partial t} [(h * f_r(\cdot, \theta, s))(t)] = \left(h * \frac{\partial}{\partial t} f_r(\cdot, \theta, s) \right)(t) \quad (96)$$

and the linearity of the inverse Radon transform [31]. The odd signal part

$$\begin{aligned} f_v^o(z, s) &= (h^{(1)} * f_v^e(\cdot, s))(\phi_v(z, s)) \\ &= a_v(z, s) \sin \phi_v(z, s) \end{aligned} \quad (97)$$

results from the even signal part

$$f_v^e(z, s) = a_v(z, s) \cos \phi_v(z, s) \quad (98)$$

by the classical 1D Hilbert transform and

$$f_v^{(m)}(z, s) = \begin{cases} f_v^e(z, s), & m \bmod 4 = 0 \\ f_v^o(z, s), & m \bmod 4 = 1 \\ -f_v^e(z, s), & m \bmod 4 = 2 \\ -f_v^o(z, s), & m \bmod 4 = 3 \end{cases} \quad (99)$$

In case of the zeroth order Hilbert transform (i.e. $i + j = 0$), this results in the local signal value $f_p(z, s)$. According to (95), the first and second order generalized Hilbert transformed signal determines the following system of linear equations

$$\begin{bmatrix} f_x \\ f_y \end{bmatrix}(z, s) = \sum_{v=1}^n \begin{bmatrix} \cos \theta_v(z, s) \\ \sin \theta_v(z, s) \end{bmatrix} f_v^o(z, s) \quad (100)$$

and

$$\begin{bmatrix} f_{xx} \\ f_{xy} \\ f_{yy} \end{bmatrix}(z, s) = \sum_{v=1}^n \begin{bmatrix} \cos^2 \theta_v(z, s) \\ \cos \theta_v(z, s) \sin \theta_v(z, s) \\ \sin^2 \theta_v(z, s) \end{bmatrix} f_v^e(z, s) \quad (101)$$

from which the signal value can be reconstructed by

$$f_p(z, s) = \sum_{v=1}^n f_v^e(z, s) = f_{xx}(z, s) + f_{yy}(z, s). \quad (102)$$

With (95), the third order Hilbert transformed signal determines the following system of linear equations

$$\begin{bmatrix} f_{xxx} \\ f_{xxy} \\ f_{xyy} \\ f_{yyy} \end{bmatrix} (z, s) = \sum_{\nu=1}^n \begin{bmatrix} \cos^3 \theta_\nu(z, s) \\ \cos^2 \theta_\nu(z, s) \sin \theta_\nu(z, s) \\ \cos \theta_\nu(z, s) \sin^2 \theta_\nu(z, s) \\ \sin^3 \theta_\nu(z, s) \end{bmatrix} f_\nu^o(z, s) \tag{103}$$

from which the first order generalized Hilbert transform can be reconstructed by

$$\begin{bmatrix} f_x \\ f_y \end{bmatrix} (z, s) = \begin{bmatrix} f_{xxx}(z, s) + f_{xyy}(z, s) \\ f_{xxy}(z, s) + f_{yyy}(z, s) \end{bmatrix}. \tag{104}$$

Due to the important relation of the Radon transform to the generalized Hilbert transform of any order, it is possible to result in a system of equations which can now be solved for the unknown signal parameters. Please note that neither the Radon transform nor its inverse are ever applied to the signal in practise. This is a very important advantage compared to the wavelet transforms, e.g. Ridgelet wavelet transforms [24]. Those approaches try out only a finite number of directions by the discrete Radon transform [24], which suffers from numerical problems. The resulting disadvantages are inaccuracy, problems resulting from aliasing effects, and higher computational time complexities.

4.4 Algebraic Signal Representation

We will now take full advantage of the results of Sect. 3.3. For the sake of simplicity, we will restrict this work to the algebra of quaternions \mathbb{H} , which are sufficient for constructing the signal tensor. Loosely spoken, simply consider the tensor-valued signal extension as a real-valued $2 \times 2 \times 3$ array. According to [27], an isomorphic mapping

$$\varphi : M(2, \mathbb{G}\mathbb{A}_3) \mapsto \mathbb{G}\mathbb{A}_{4,1} \tag{105}$$

from the quaternion-valued tensor

$$T = T^e + T_x^o \mathbf{i} + T_y^o \mathbf{j} \tag{106}$$

to the quaternion-valued vector

$$\varphi(T) = \varphi(T^e) + \varphi(T_x^o) \mathbf{i} + \varphi(T_y^o) \mathbf{j} \tag{107}$$

is possible. With the set of basis elements

$$\{1, \mathbf{i}, \mathbf{j}, \mathbf{k}\} \tag{108}$$

of the quaternions $(\mathbb{H}, +, \circ)$ with

$$\mathbb{H} = \{q_s + q_i \mathbf{i} + q_j \mathbf{j} + q_k \mathbf{k} : q_s, q_i, q_j, q_k \in \mathbb{R}\} \tag{109}$$

and the isomorphisms

$$\mathbf{i} \cong \mathbf{e}_{13}, \quad \mathbf{j} \cong \mathbf{e}_{23}, \quad \mathbf{k} \cong \mathbf{e}_{21} \tag{110}$$

with $\mathbf{i} \circ \mathbf{j} = \mathbf{k}$, the signal tensor for $n < 3$ in (82) can be defined by the generalized Hilbert transforms of second order (T^e) and third order (T_x^o and T_y^o)

$$T = \underbrace{\begin{bmatrix} f_{xx} & f_{xy} \\ f_{xy} & f_{yy} \end{bmatrix}}_{T^e} + \underbrace{\begin{bmatrix} f_{xxx} & f_{xxy} \\ f_{xxy} & f_{xyy} \end{bmatrix}}_{T_x^o} \mathbf{i} + \underbrace{\begin{bmatrix} f_{xxy} & f_{xyy} \\ f_{xyy} & f_{yyy} \end{bmatrix}}_{T_y^o} \mathbf{j}, \tag{111}$$

see Fig. 14. By introducing the abbreviations

$$f^-(z, s) = f_{xx}(z, s) - f_{yy}(z, s) = \sum_{\nu=1}^n \cos(2\theta_\nu(z, s)) f_\nu^e(z, s), \tag{112}$$

$$f_x^-(z, s) = f_{xxx}(z, s) - f_{xyy}(z, s), \tag{113}$$

$$f_y^-(z, s) = f_{xxy}(z, s) - f_{yyy}(z, s) \tag{114}$$

the quaternion-valued matrix T can be mapped by the isomorphism φ , with the same treatment like in (52), to a quaternion-valued multi-vector representation [31] in conformal space $\mathbb{G}\mathbb{A}_{4,1}$ [25]

$$\begin{aligned} \varphi(T(z, s)) &= \varphi(T^e(z, s)) + \varphi(T_x^o(z, s)) \mathbf{i} + \varphi(T_y^o(z, s)) \mathbf{j} \\ &= \left[\frac{f_p(z, s)}{2} + f_{xy}(z, s) \mathbf{e}_+ + \frac{f^-(z, s)}{2} \mathbf{e}_{+-} \right] \\ &\quad + \left[\frac{f_x(z, s)}{2} + f_{xxy}(z, s) \mathbf{e}_+ + \frac{f_x^-(z, s)}{2} \mathbf{e}_{+-} \right] \mathbf{i} \\ &\quad + \left[\frac{f_y(z, s)}{2} + f_{xyy}(z, s) \mathbf{e}_+ + \frac{f_y^-(z, s)}{2} \mathbf{e}_{+-} \right] \mathbf{j} \end{aligned} \tag{115}$$

which will be called signal multi-vector, see Fig. 15. Compare the signal multi-vector with the structure multi-vector [6], and the more common Weyl-projection operator [29] induced by

$$\left(\mathcal{H}^{(1)}\{(p_s * f)\}, \mathcal{H}^{(2)}\{(p_s * f)\}, \mathcal{H}^{(3)}\{(p_s * f)\} \right). \tag{116}$$

Compared to the structure multi-vector the signal multi-vector has less restrictions concerning the signal model. And compared to the Weyl-projection⁶ the signal multi-vector is

⁶We thank one of the reviewers for the hint that the proposed multi-vector structure has some similarities, but delivers a different result,

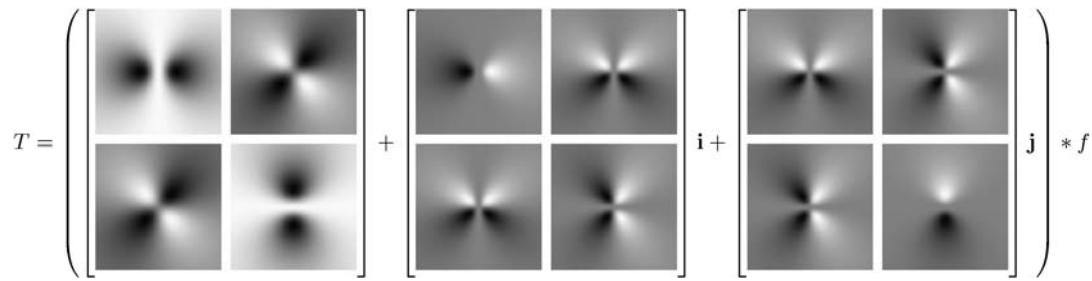


Fig. 14 Illustration of the convolution kernels in the spatial domain of the quaternion-valued matrix signal representation T

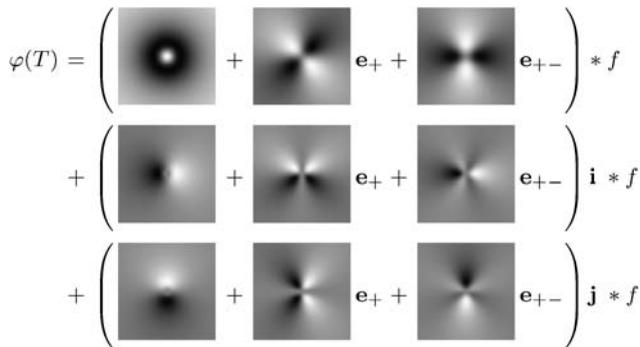


Fig. 15 Illustration of the convolution kernels in the spatial domain of the signal multi-vector $\varphi(T)$ which is defined in (115)

an alternative signal representation. The signal multi-vector delivers the complete geometrical and structural information of the assumed signal model (82). In [3] the geometrical signal features have been retrieved by higher order derivatives in the traditional matrix expression. This is generalized by $\varphi(T)$ in a more natural embedding.

4.5 Geometry from the Signal Multi-Vector

The hardest challenge in signal analysis is to obtain exact geometrical signal features such as the orientations $\theta_v(z, s)$. The most important relations are

$$\sin(2\theta_{2/1}(z, s)) = \frac{\det \begin{bmatrix} f_{xxy}(z, s) \cos \theta_{1/2}(z, s) \\ f_{xyy}(z, s) \sin \theta_{1/2}(z, s) \end{bmatrix}}{\det D_{1/2}} \tag{117}$$

and

$$\cos(2\theta_{2/1}(z, s)) = \frac{\det \begin{bmatrix} \frac{f_x^-(z, s)}{2} \cos \theta_{1/2}(z, s) \\ \frac{f_y^-(z, s)}{2} \sin \theta_{1/2}(z, s) \end{bmatrix}}{\det D_{1/2}} \tag{118}$$

with the application of the Weyl-projection operator on tensor-field representations of an image for detecting orientational symmetries.

with the matrix

$$D_{1/2} = \begin{bmatrix} \frac{f_x(z, s)}{2} & \cos \theta_{1/2}(z, s) \\ \frac{f_y(z, s)}{2} & \sin \theta_{1/2}(z, s) \end{bmatrix} \tag{119}$$

which follow from (103) of the third order generalized Hilbert transform and (100) of the first order generalized Hilbert transform for $n = 2$ (note that the derivation is not trivial). From the fact that

$$\sin^2(2\theta_{2/1}(z, s)) + \cos^2(2\theta_{2/1}(z, s)) = 1, \tag{120}$$

the nonlinear part of the inverse problem follows in form of a quadratic equation

$$\gamma^-(z, s) \sin^2 \theta_v(z, s) + \alpha(z, s) \sin(2\theta_v(z, s)) = \beta(z, s), \tag{121}$$

since two unknown orientations have to satisfy the equation. With the known values given by the geometric product \circ of the two odd parts

$$\varphi(T_x^o(z, s)) \circ \varphi(T_x^o(z, s)) \in \mathbb{GA}_{4,1}, \tag{122}$$

$$\varphi(T_x^o(z, s)) \circ \varphi(T_y^o(z, s)) \in \mathbb{GA}_{4,1}, \tag{123}$$

$$\varphi(T_y^o(z, s)) \circ \varphi(T_y^o(z, s)) \in \mathbb{GA}_{4,1} \tag{124}$$

the following elements are being constructed by the geometric product of the corresponding Clifford algebra

$$\delta(z, s) = \left[\frac{f_x(z, s)}{2} \right]^2 - f_{xxy}^2(z, s) - \left[\frac{f_x^-(z, s)}{2} \right]^2, \tag{125}$$

$$\beta(z, s) = \left[\frac{f_y(z, s)}{2} \right]^2 - f_{xyy}^2(z, s) - \left[\frac{f_y^-(z, s)}{2} \right]^2, \tag{126}$$

$$\alpha(z, s) = \frac{f_x(z, s)}{2} \frac{f_y(z, s)}{2} - f_{xxy}(z, s) f_{xyy}(z, s) - \frac{f_x^-(z, s)}{2} \frac{f_y^-(z, s)}{2}. \tag{127}$$

Let be

$$\gamma^+(z, s) = \beta(z, s) + \delta(z, s), \tag{128}$$

Table 1 Evolution of the classical analytic signal with $z = (x, y)$ and $\bar{\sigma}_v = [\cos \theta_v, \sin \theta_v]^T$

	Signal Model	Domain	Algebra	Geometry
1D Analytic Signal	$f(x, s) = a(x, s) \cos(x + \phi(x, s))$	1D	\mathbb{C}	Euclidean space
2D Monogenic Signal	$f(z, s) = a(z, s) \cos(\langle z, \bar{\sigma} \rangle + \phi(z, s))$	i1D	\mathbb{R}^3	Euclidean space
2D Analytic Signal	$f(z, s) = a(z, s) \sum_{v=1}^2 \cos(\langle z, \bar{\sigma}_v(z, s) \rangle + \phi(z, s))$	i1D \cup i2D	$\mathbb{GA}_{4,1}$	Projective space
Signal Multi-Vector	$f(z, s) = \sum_{v=1}^n a_v(z, s) \cos(\langle z, \bar{\sigma}_v \rangle + \phi_v(z, s))$	2D	HMGA	Conformal space

$$\gamma^-(z, s) = \beta(z, s) - \delta(z, s). \tag{129}$$

Due to the elements being constructed by the geometric product the main orientation can be derived by

$$\theta_1(z, s) + \theta_2(z, s) = \arctan \frac{2\alpha(z, s)}{\gamma^-(z, s)} \tag{130}$$

as well as the apex angle

$$|\theta_1(z, s) - \theta_2(z, s)| = \arctan \frac{2\sqrt{\alpha^2(z, s) - \beta(z, s)\delta(z, s)}}{\gamma^+(z, s)} \tag{131}$$

from which the single orientations $\theta_v(z)$ can be obtained.

Although Clifford algebra is not necessary for the solution presented in this work, the application of the geometric product delivers easily a compact access to the geometric features hidden in the chosen signal representation.

4.6 Structure from the Signal Multi-Vector

The phase and the amplitude represent the structural signal features, which can be calculated by solving a linear system of equations by Cramer’s rule for 2×2 matrices. The even and odd signal parts can be written as

$$\begin{bmatrix} f_1^e(z, s) \\ f_2^e(z, s) \end{bmatrix} = \frac{1}{c^e(z, s)} \begin{bmatrix} \frac{f_p(z, s)}{2} \sin(2\theta_2(z, s)) - f_{xy}(z, s) \\ f_{xy}(z, s) - \frac{f_p(z, s)}{2} \sin(2\theta_1(z, s)) \end{bmatrix} \tag{132}$$

which has been derived by the second order generalized Hilbert transform in (101) with

$$c^e(z, s) = \sin(\theta_1(z, s) - \theta_2(z, s)) \times \cos(\theta_1(z, s) + \theta_2(z, s)) \tag{133}$$

and

$$\begin{bmatrix} f_1^o(z, s) \\ f_2^o(z, s) \end{bmatrix} = \frac{1}{c^o(z, s)}$$

$$\times \begin{bmatrix} f_y(z, s) \cos \theta_2(z, s) - f_x(z, s) \sin \theta_2(z, s) \\ f_x(z, s) \sin \theta_1(z, s) - f_y(z, s) \cos \theta_1(z, s) \end{bmatrix} \tag{134}$$

which has been derived by the first order generalized Hilbert transform in (100) respectively with

$$c^o(z, s) = \sin(\theta_1(z, s) - \theta_2(z, s)). \tag{135}$$

By means of the even and odd signal parts, finally structural signal features such as the phases and the amplitudes can be derived as

$$\phi_v(z, s) = \arctan \frac{f_v^o(z, s)}{f_v^e(z, s)} \tag{136}$$

and

$$a_v(z, s) = \sqrt{(f_v^e(z, s))^2 + (f_v^o(z, s))^2} \tag{137}$$

for $v \in \{1, 2\}$. Interestingly, this solution corresponds for each signal component to the classical 1D analytic signal [11], please refer to (10) and (11).

5 Conclusion

We have solved a fundamental problem of isotropic 2D signal analysis by introducing a novel algebraic image signal representation, which can be used for interpretation and powerful feature extraction without steering. All results can be proved by real-valued trigonometric calculations which can be avoided by basic calculations in geometric algebra using the geometric product. Our novel approach can be described for arbitrary signal models by the following general steps

1. Signal modeling in scale space and signal extension by the generalized Hilbert transform. The order of the required generalized Hilbert transforms correlates to the complexity n of the signal model in (82).
2. Retrieving the explicit system of equations including all unknown signal parameters (θ_v, ϕ_v, a_v) by the relation of the generalized Hilbert transform to the Radon transform.
3. Algebraic signal representation in tensor form and subsequent mapping by the isomorphism φ to its corresponding signal multi-vector.

- 4. Geometric interpretation of the signal multi-vector by solving the nonlinear part of the inverse problem.
- 5. Structural multi-vector-valued signal interpretation by solving the linear part of the inverse problem.

The message of this contribution is that truly isotropic signal analysis is possible which offers best accuracy in less computational time complexity. Future work will contain the generalization of the signal multi-vector to multidimensional signal domains to enable also isotropic motion tracking in computer vision applications, as well as providing the basic theory for truly isotropic wavelet analysis [28]. The evolution of the generalization of the analytic signal can be seen in Table 1.

Acknowledgements We acknowledge funding by the German Research Foundation (DFG) under the project *SO 320/4-2* and a special thank to both of the reviewers for the interesting hints and detailed advice.

Appendix A: Spatial Second Order Generalized Hilbert Transform Kernels in Poisson Scale Space

Proof To calculate the convolution in frequency space, the Fourier transforms $\mathcal{F}\{\cdot\}(u)$ of the convolution kernels $h^{(2)}(z)$ and $p(z, s)$ are considered. According to the convolution theorem, the convolution in the spatial domain corresponds to a multiplication in Fourier space. The Fourier transform of $h^{(2)}(z)$ results in the multiplier

$$\mathcal{F}\{h^{(2)}\}(u) = -\frac{\bar{u}}{u} \tag{138}$$

with

$$u = u_1 + \mathbf{i}u_2 \in \mathbb{C} \tag{139}$$

and the conjugate

$$\bar{u} = u_1 - \mathbf{i}u_2. \tag{140}$$

The Fourier transform of the Poisson convolution kernel $p(z, s)$ is obtained as

$$\mathcal{F}\{p\}(u; s) = e^{-2\pi\|u\|s}. \tag{141}$$

By representing the frequency domain in polar coordinates, with

$$u = r[\cos\theta + \mathbf{i}\sin\theta] \tag{142}$$

and

$$z = x + \mathbf{i}y = k[\cos\varphi + \mathbf{i}\sin\varphi], \tag{143}$$

the frequency transfer functions of these kernels read

$$\mathcal{F}\{h^{(2)}\}(u) = -\frac{e^{-\mathbf{i}\theta}}{e^{\mathbf{i}\theta}} = -e^{-\mathbf{i}2\theta} \tag{144}$$

and

$$\mathcal{F}\{p_s\}(u) = e^{-2\pi rs}. \tag{145}$$

Using the polar coordinate representation of the inverse two-dimensional Fourier transform to obtain the spatial domain representation of the kernels yields

$$\begin{aligned} (p_s * h^{(2)})(z) &= \mathcal{F}^{-1}\{-e^{-2\pi rs} e^{-\mathbf{i}2\theta}\}(z) \\ &= 2\pi \int_{r=0}^{\infty} \int_{\theta=0}^{2\pi} -e^{-2\pi rs} e^{-\mathbf{i}2\theta} e^{\mathbf{i}2\pi kr \cos(\theta-\varphi)} r \, d\theta \, dr \\ &= 2\pi \int_{r=0}^{\infty} \int_{\theta=0}^{2\pi} -e^{-2\pi rs} \\ &\quad \times e^{-\mathbf{i}2(\theta+\varphi)} e^{\mathbf{i}2\pi kr \cos(\theta-\varphi+\varphi)} r \, d\theta \, dr \\ &= -2\pi e^{-\mathbf{i}2\varphi} \int_{r=0}^{\infty} e^{-2\pi rs} \\ &\quad \times \underbrace{\left[\int_{\theta=0}^{2\pi} e^{-\mathbf{i}2\theta} e^{-\mathbf{i}2\pi kr \cos\theta} \, d\theta \right]}_{=J_2(2\pi kr)} r \, dr \\ &= -2\pi e^{-\mathbf{i}2\varphi} \int_{r=0}^{\infty} e^{-2\pi rs} J_2(2\pi kr) r \, dr \end{aligned} \tag{146}$$

where J_2 is a Bessel function of the first kind and second order. In the following the abbreviations $\alpha = 2\pi s$ and $\beta = 2\pi k$ will be used. J_2 can be written according to the recurrence relation for Bessel functions as

$$J_2(2\pi kr) = J_2(\beta r) = \frac{2}{\beta r} J_1(\beta r) - J_0(\beta r) \tag{147}$$

since the recurrence relation reads

$$J_\nu(x) = \frac{2(\nu - 1)}{x} J_{\nu-1}(x) - J_{\nu-2}(x). \tag{148}$$

These results lead to

$$\begin{aligned} (h^{(2)} * p_s)(z) &= -2\pi e^{-\mathbf{i}2\varphi} \int_{r=0}^{\infty} e^{-\alpha r} J_2(2\pi kr) r \, dr \\ &= -2\pi e^{-\mathbf{i}2\varphi} \int_{r=0}^{\infty} e^{-\alpha r} \frac{2}{\beta r} J_1(\beta r) r \, dr \\ &\quad + 2\pi e^{-\mathbf{i}2\varphi} \int_{r=0}^{\infty} e^{-\alpha r} J_0(\beta r) r \, dr \\ &= -2\pi e^{-\mathbf{i}2\varphi} \left[\frac{2}{\beta} \int_{r=0}^{\infty} e^{-\alpha r} J_1(\beta r) dr \right] \end{aligned}$$

$$- \int_{r=0}^{\infty} e^{-\alpha r} J_0(\beta r) r \, dr \Big]. \tag{149}$$

According to common integral tables [12] one obtains the evaluation of the two Bessel integrals as

$$\frac{2}{\beta} \int_{r=0}^{\infty} e^{-\alpha r} J_1(\beta r) \, dr = \frac{2[\sqrt{\alpha^2 + \beta^2} - \alpha]}{\beta^2 \sqrt{\alpha^2 + \beta^2}} \tag{150}$$

since

$$\int_{r=0}^{\infty} e^{-\alpha r} J_\nu(\beta r) \, dr = \frac{[\sqrt{\alpha^2 + \beta^2} - \alpha]^\nu}{\beta^\nu \sqrt{\alpha^2 + \beta^2}} \tag{151}$$

and

$$\int_{r=0}^{\infty} e^{-\alpha r} J_0(\beta r) r \, dr = \frac{2\alpha \Gamma(\frac{3}{2})}{\sqrt{\pi}(\alpha^2 + \beta^2)^{\frac{3}{2}}} = \frac{\alpha}{(\alpha^2 + \beta^2)^{\frac{3}{2}}} \tag{152}$$

since $\Gamma(\frac{3}{2}) = \frac{\sqrt{\pi}}{2}$ and

$$\int_{r=0}^{\infty} e^{-\alpha r} J_\nu(\beta r) r^{\nu+1} \, dr = \frac{2\alpha(2\beta)^\nu \Gamma(\nu + \frac{3}{2})}{\sqrt{\pi}(\alpha^2 + \beta^2)^{\nu + \frac{3}{2}}}. \tag{153}$$

Plugging these results in the equations above results in

$$\begin{aligned} (h^{(2)} * p_s)(z) &= -2\pi e^{-i2\varphi} \int_{r=0}^{\infty} e^{-\alpha r} J_2(2\pi kr) r \, dr \\ &= \frac{s(2s^2 + 3\|z\|^2) - 2(s^2 + \|z\|^2)^{\frac{3}{2}}}{2\pi \|z\|^4 (s^2 + \|z\|^2)^{\frac{3}{2}}} (x^2 - 2ixy - y^2) \end{aligned} \tag{154}$$

with

$$\begin{aligned} e^{-i2\varphi} &= [e^{-i\varphi}]^2 = \left[\frac{\bar{z}}{\|z\|} \right]^2 \\ &= \frac{(x - iy)^2}{\|z\|^2} = (x^2 - 2ixy - y^2) \frac{1}{\|z\|^2}. \end{aligned} \tag{155}$$

These results lead to the three different 2D convolution kernels in the spatial domain of the second order generalized Hilbert transform in Poisson scale space

$$q^{(2)}(z, s) = \frac{3s\|z\|^2 + 2s^3 - 2(\|z\|^2 + s^2)^{\frac{3}{2}}}{2\pi \|z\|^4 (\|z\|^2 + s^2)^{\frac{3}{2}}} \begin{bmatrix} x^2 \\ xy \\ y^2 \end{bmatrix}. \tag{156}$$

□

Appendix B: Appendix: Spatial Third Order Generalized Hilbert Transform Kernels in Poisson Scale Space

Proof The Fourier transform of the convolution kernel $h^{(3)}(x, y)$ results in the multiplier

$$\mathcal{F}\{h^{(3)}\}(u) = -e^{-i3\theta}. \tag{157}$$

In the same way as for the second order Hilbert transform we now compute the representation of the third order Hilbert transform in monogenic scale space.

$$\begin{aligned} (h^{(3)} * p_s)(z) &= \mathcal{F}^{-1}\{-e^{-2\pi rs} e^{-i3\theta}\}(z) \\ &= 2\pi \int_{r=0}^{\infty} \int_{\theta=0}^{2\pi} -e^{-2\pi rs} e^{-i3\theta} e^{i2\pi kr \cos(\theta-\varphi)} r \, d\theta \, dr \\ &= 2\pi \int_{r=0}^{\infty} \int_{\theta=0}^{2\pi} -e^{-2\pi rs} \\ &\quad \times e^{-i3(\theta+\varphi)} e^{i2\pi kr \cos(\theta-\varphi+\varphi)} r \, d\theta \, dr \\ &= -2\pi e^{-i3\varphi} \int_{r=0}^{\infty} e^{-2\pi rs} \\ &\quad \times \underbrace{\left[\int_{\theta=0}^{2\pi} e^{-i3\theta} e^{-i2\pi kr \cos \theta} \, d\theta \right]}_{=J_3(2\pi kr)} r \, dr \\ &= -2\pi e^{-i3\varphi} \int_{r=0}^{\infty} e^{-2\pi rs} J_3(2\pi kr) r \, dr \end{aligned} \tag{158}$$

with

$$J_3(2\pi kr) = J_3(\beta r) = \frac{4}{\beta r} J_2(\beta r) - J_1(\beta r) \tag{159}$$

and with

$$\int_{r=0}^{\infty} e^{-\alpha r} J_\nu(\beta r) r^\nu \, dr = \frac{(2\beta)^\nu \Gamma(\nu + \frac{1}{2})}{\sqrt{\pi}(\alpha^2 + \beta^2)^{\nu + \frac{1}{2}}}. \tag{160}$$

The 2D convolution kernels in the spatial domain of the third order Hilbert transform in monogenic scale space read

$$\begin{aligned} q^{(3)}(z, s) &= \frac{4s^2(2s^2 + 3\|z\|^2) + 3\|z\|^4 - 8s(s^2 + \|z\|^2)^{3/2}}{2\pi \|z\|^6 (s^2 + \|z\|^2)^{3/2}} \\ &\quad \times \begin{bmatrix} x^3 \\ x^2y \\ xy^2 \\ y^3 \end{bmatrix}. \end{aligned} \tag{161}$$

□

□

References

1. Bülrow, T., Sommer, G.: Hypercomplex signals—a novel extension of the analytic signal to the multidimensional case. *IEEE Trans. Signal Process.* **49**(11), 2844–2852 (2001)
2. Carneiro, G., Jepson, A.D.: Phase-based local features. In: 7th European Conference on Computer Vision—Part I. LNCS, vol. 2350, pp. 282–296. Springer, Berlin (2002)
3. Danielsson, P.E., Lin, Q., Ye, Q.Z.: Efficient detection of second-degree variations in 2D and 3D images. *J. Vis. Commun. Image Represent.* **12**(3), 255–305 (2001)
4. Delanghe, R.: Clifford analysis: History and perspective. *Comput. Methods Funct. Theory* **1**(1), 107–153 (2001)
5. Delanghe, R.: On some properties of the Hilbert transform in Euclidean space. *Bull. Belg. Math. Soc. Simon Stevin* **11**(2), 163–180 (2004)
6. Felsberg, M.: Low-level image processing with the structure multivector. Technical Report 2016, Kiel University, Department of Computer Science (2002)
7. Felsberg, M., Sommer, G.: The monogenic signal. *IEEE Trans. Signal Process.* **49**(12), 3136–3144 (2001)
8. Felsberg, M., Sommer, G.: The monogenic scale-space: A unifying approach to phase-based image processing in scale-space. *J. Math. Imaging Vis.* **21**, 5–26 (2004)
9. Fleet, D.J., Jepson, A.D.: Stability of phase information. *IEEE Trans. Pattern Anal. Mach. Intell.* **15**(12), 1253–1268 (1993)
10. Fleet, D.J., Jepson, A.D., Jenkin, M.R.M.: Phase-based disparity measurement. *CVGIP: Image Underst.* **53** (1991)
11. Gabor, D.: Theory of communication. *J. IEE Lond.* **93**(26), 429–457 (1946)
12. Gradshteyn, I.S., Ryzhik, I.M.: Table of Integrals, Series, and Products. Academic Press, San Diego (2007)
13. Granlund, G.H., Knutsson, H.: Signal Processing for Computer Vision. Kluwer Academic, Dordrecht (1995)
14. Grau, V., Becher, H., Alison, Noble J.: Registration of multiview real-time 3-d echocardiographic sequences. In: MICCAI (1), pp. 612–619 (2006)
15. Grau, V., Noble, J.A.: Adaptive multiscale ultrasound compounding using phase information. In: MICCAI, pp. 589–596 (2005)
16. Hahn, S.L.: Hilbert Transforms in Signal Processing. Artech House, Boston (1996)
17. Hestenes, D., Sobczyk, G.: Clifford Algebra to Geometric Calculus, a Unified Language for Mathematics and Physics. Fundamental Theories of Physics. Kluwer Academic, Dordrecht (1999)
18. Huang, T., Burnett, J., Deczky, A.: The importance of phase in image processing filters. *IEEE Trans. Acoust. Speech Signal Process.* **23**(6), 529–542 (1975)
19. Jähne, B.: Digital Image Processing. Springer, Berlin (2001)
20. Köthe, U., Felsberg, M.: Riesz-transforms vs. derivatives: On the relationship between the boundary tensor and the energy tensor. In: Kimmel, R., Sochen, N., Weickert, J. (eds.) Scale Space and PDE Methods in Computer Vision. LNCS, vol. 3459, pp. 179–191. Springer, Berlin (2005)
21. Larkin, K.G.: Natural Demodulation of 2D Fringe Patterns (2001)
22. Lowe, D.G.: Distinctive image features from scale-invariant keypoints. *Int. J. Comput. Vis.* **60**, 91–110 (2004)
23. Oppenheim, A.V., Lim, J.S.: The importance of phase in signals. *Proc. IEEE* **69**(5), 529–541 (1981)
24. Pan, W., Bui, T.D., Suen, C.Y.: Rotation invariant texture classification by ridgelet transform and frequency-orientation space decomposition. *Signal Process.* **88**(1), 189–199 (2008)
25. Perwass, C.: Geometric Algebra with Applications in Engineering. Geometry and Computing, vol. 4. Springer, Berlin (2009)
26. Rieger, B., van Vliet, L.J.: Representing orientation in n -dimensional spaces. In: CAIP. LNCS, vol. 2756, pp. 17–24. Springer, Berlin (2003)
27. Sobczyk, G., Erlebacher, G.: Hybrid matrix geometric algebra. In: Li, H., Olver, P.J., Sommer, G. (eds.) Computer Algebra and Geometric Algebra with Applications. LNCS, vol. 3519, pp. 191–206. Springer, Berlin (2005)
28. Unser, M., Balać, K., Van De Ville, D.: The monogenic Riesz-Laplace wavelet transform. In: Proceedings of the Sixteenth European Signal Processing Conference (EUSIPCO'08) (2008)
29. Weyl, H.: The Theory of Groups and Quantum Mechanics. Dover, New York (1928)
30. Wietzke, L., Fleischmann, O., Sommer, G.: 2D image analysis by generalized Hilbert transforms in conformal space. In: ECCV (2). LNCS, vol. 5303, pp. 638–649. Springer, Berlin (2008)
31. Wietzke, L., Sommer, G.: The 2D analytic signal. Technical Report 0802, Kiel University, Department of Computer Science (2008)
32. Wietzke, L., Sommer, G.: The conformal monogenic signal. In: Rigoll, G. (ed.) DAGM, Pattern Recognition. LNCS, vol. 5096, pp. 527–536. Springer, Berlin (2008)
33. Wietzke, L., Sommer, G.: The relation of inverse problems and isotropic 2D signal analysis. In: Mathematics in Signal Processing 8. Institute of Mathematics and its Applications (2008)
34. Wietzke, L., Sommer, G., Fleischmann, O.: The geometry of 2D image signals. In: CVPR 2009, pp. 1690–1697. IEEE Computer Society on Computer Vision and Pattern Recognition (2009)
35. Xiaoxun, Z., Yunde, J.: Local steerable phase (lsp) feature for face representation and recognition. In: CVPR '06: Proceedings of the 2006 IEEE Computer Society Conference on Computer Vision and Pattern Recognition, pp. 1363–1368. IEEE Computer Society, Los Alamitos (2006)
36. Zang, D., Wietzke, L., Schmaltz, C., Sommer, G.: Dense optical flow estimation from the monogenic curvature tensor. In: Scale Space and Variational Methods. LNCS, vol. 4485, pp. 239–250. Springer, Berlin (2007)
37. Zetsche, C., Barth, E.: Fundamental limits of linear filters in the visual processing of two-dimensional signals. *Vis. Res.* **30**, 1111–1117 (1990)